



## Controllable preparation of hierarchical NiO hollow microspheres with high pseudo-capacitance

Hong-zhi YANG, Jian-peng ZOU

State Key Laboratory of Powder Metallurgy, Central South University, Changsha 410083, China

Received 24 April 2017; accepted 5 September 2017

**Abstract:** Nickel oxide (NiO) hollow microspheres with hierarchical structure were fabricated through a process consisting of a self-assembling, hydrothermal reaction and calcination. The prepared NiO hollow microspheres composed of many nanoflakes, are about 2–3  $\mu\text{m}$  in diameter. The length of the NiO flakes, having clear edges, is about 500–700 nm, while the thickness is only about 40–50 nm. This indicates that the NiO microspheres possess a hierarchical structure that can provide porous channels to facilitate the transmission of both electrons and electrolyte ions. NiO microspheres exhibit a high specific capacitance of about 1340 F/g at a current density of 1 A/g and high capacitance retention about 96.5% after 1000 cycles. What's more, the conductive mechanism of nickel oxide for electrochemical capacitor electrodes was also studied.

**Key words:** nickel oxide hollow microsphere; hierarchical structure; controllable preparation; self-assembling; pseudo-capacitance

### 1 Introduction

The issues of energy resources and their impact on the environment have become more and more prominent with the development of modern society and the growth of the population. Energy sources currently available hardly meet the high power and energy densities required by both conventional secondary batteries and traditional capacitors. Supercapacitors have attracted worldwide attention because of their higher power density and longer cycle life than conventional secondary batteries, as well as higher energy density compared with conventional capacitors [1], which have been widely used in a variety of areas, such as portable electronics, backup power sources and military devices [2–4].

Ruthenium oxide ( $\text{RuO}_2$ ) has been widely studied as an electrode for pseudo capacitors due to its great conductivity, reversible redox process and high specific capacitance [5,6], which favor the development of high energy and power densities in electrochemical capacitors. The extensive use of  $\text{RuO}_2$  is limited by its high cost. However, nickel oxide (NiO), which has a high theoretical specific capacitance of 2584 F/g [7], environmental compatibility, high chemical and thermal stability,

practical availability and lower cost, should be an optimal alternative material for pseudo capacitors [8,9]. The morphology and microstructure of NiO are very important to improve its pseudo-capacitance, so many efforts have been devoted to the synthesis of NiO nano-materials by applying various wet chemical methods to obtain different morphologies, such as nanoparticles [10], nanoplates [10–13], hollow octahedrons [14] and complicated hierarchical nanostructures [15,16]. However, the real specific capacitance obtained from NiO materials [17–23] is still far below its theoretical value because of its relatively high resistances (0.01–0.35 S/cm at room temperature [24]).

As a material for electrochemical capacitor electrodes, hierarchical NiO hollow microspheres can achieve high specific capacitance, high porosity as well as many open channels because of its special structure, which is helpful to improve the specific capacity of NiO material. Lysine is a special surface active agent and has many functional groups and special structure, which can be used as a very effective self-assembly reagent to play an important role in the growth of the material [25]. In this work, we report a facile fabrication route to synthesize hierarchical NiO hollow microspheres through self-assembling, hydrothermal reaction and

calcination using lysine as structure regulator. Notably, the fabrication route is facile and efficient, suited for both laboratory and large-scale operations. A schematic description of the synthesis procedure was also illustrated. Meanwhile, we also study the conductive mechanism of nickel oxide, used as material for electrochemical capacitor electrodes.

## 2 Experimental

### 2.1 Preparation of hierarchical NiO hollow microspheres

The fabrication route of NiO hollow microspheres with hierarchical structure is shown schematically in Fig. 1. Biologically pure lysine was used, while the other reagents were analytically pure and used without further purification. In a typical process, green nickel chloride ( $\text{NiCl}_2 \cdot 6\text{H}_2\text{O}$ ) particles were dissolved in deionized water and the solution was homogenized by vigorous stirring for 30 min. The  $\text{NiCl}_2$  solution was then mixed with lysine powder and stirred for 30 min until it turned pale blue. Afterwards, ammonium hydroxide was dropped into the  $\text{NiCl}_2$ /lysine solution, whose color was transformed slowly to navy blue. About 30 min was required to drop the necessary amount of ammonium hydroxide, after which the solution was further stirred for 30 min, placed in a Teflon lined autoclave, and heated at  $180\text{ }^\circ\text{C}$  for 6 h. After cooling to room temperature, the green precipitate was filtered, repeatedly washed with deionized water and dried overnight at  $60\text{ }^\circ\text{C}$ . Finally, the precursor of the NiO powder was calcined at  $350\text{ }^\circ\text{C}$  for 3 h in air. Black NiO hollow microspheres were obtained at the end of this process.

To investigate the growth mechanism of the NiO

microspheres, several experiments were performed using different hydrothermal reaction time. The hydrothermal reaction was conducted for 6, 8, 10, and 12 h. The obtained samples were calcined at  $350\text{ }^\circ\text{C}$  for 3 h in air to enable a comparison of their characteristics to those with different hydrothermal reaction time.

### 2.2 Structural characterization

The hierarchical NiO hollow microspheres were characterized using scanning electron microscopy (SEM, Nova Nano230, FEI, Oregon, USA), and transmission electron microscopy (TEM, JEM-2100F, JEOL Ltd., Japan). Phase analysis was carried out by X-ray diffraction (XRD) analysis (Rigaku Ltd., Japan, D/max 2550VB,  $\text{Cu K}_\alpha$  radiation, 40 kV, 250 mA). Molecular vibration behavior was investigated using a Fourier transform infrared (FTIR; Nicolet 6700, USA) in the  $4000\text{--}400\text{ cm}^{-1}$  range. Thermal analysis was also conducted with STA449C thermal analyzer (NETZSCH, Germany) to analyze the calcination process. The  $\text{N}_2$  adsorption/desorption isotherm was determined using TriStar 3020 to obtain information about the specific surface and pore structure (TriStar 3020, Micromeritics, USA).

### 2.3 Electrochemical characterization

Electrochemical characterization was performed using CHI 660E electrochemical workstation (Shanghai Chenhua Instrument Co., China) in a three-electrode system at room temperature. The working electrode was fabricated according to the following procedure. First, the obtained NiO material, acetylene black and polyvinylidene fluoride were mixed in a mass ratio of 85:5:10 and dispersed by N-methylketopyrrolidine. The

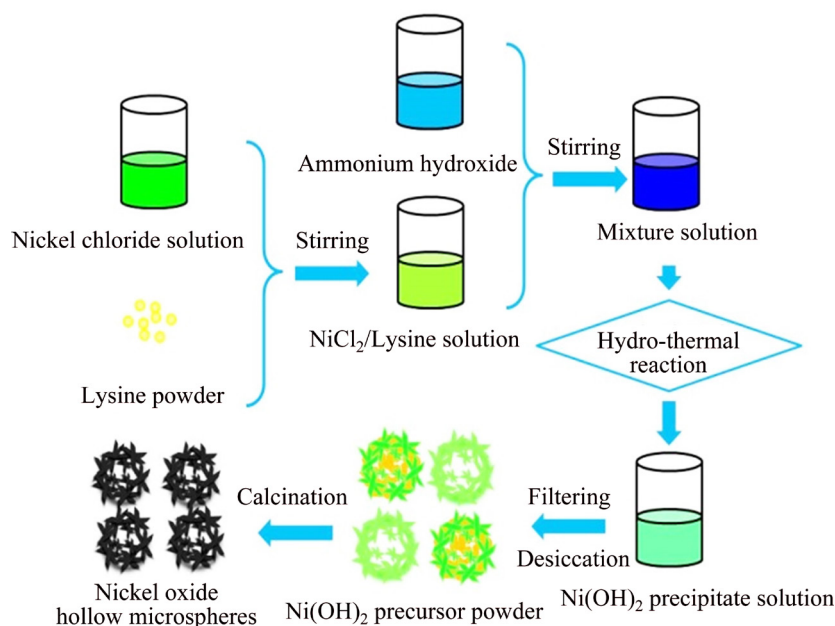


Fig. 1 Fabrication route of hierarchical NiO hollow microspheres

Ni foams were used as current collectors and treated by acetone and ethanol for 15 min, respectively. Then, the mixture was coated on Ni foams and dried at 60 °C for 12 h under vacuum condition. The mass loading in the test electrode is about 4.5 mg/cm<sup>2</sup>. Cyclic voltammetry (CV), galvanostatic charge/discharge and electrochemical impedance spectroscopy (EIS) were measured in a 6 mol/L KOH aqueous solution using platinum plate as the counter electrode and saturated calomel electrode (SCE, Hg/Hg<sub>2</sub>Cl<sub>2</sub>) as the reference electrode.

### 3 Results and discussion

#### 3.1 Structural characterization

The morphology of the prepared hierarchical NiO hollow microspheres is shown in Fig. 2. It can be seen that the NiO microspheres, composed of many nano NiO flakes, have good dispersion and are about 2–3 μm in diameter (Fig. 2(a)). In addition, as shown in Fig. 2(b), the obtained NiO sphere is hollow, with many flakes stacked and crossed to form hierarchical structure. Figure 2(c) displays the magnified image of NiO microspheres, from which more detailed information can be obtained. The length of the NiO flakes with clear edges is about 400–600 nm, while the thickness is only about 40–50 nm. Such a unique structure can provide high porosity and specific surface area as well as open channels, all of which are beneficial to the diffusion and migration of both electrolyte ions and electrons. Then, the electrolyte can be infiltrated into the NiO microspheres to improve the utilization ratio of the NiO active material. So, the capacitance of NiO can be enhanced.

The SEM images of NiO microspheres obtained after different hydrothermal reaction time are exhibited in Fig. 3. It is evident that NiO microspheres can be obtained after the 6 h treatment. All the microspheres obtained with different reaction time have similar morphology, good dispersion and uniform size. The thickness of the NiO flakes increases with the hydrothermal treatment time since the nanoflakes have a

high surface energy, which tend to evolve towards a lower energy condition through the Ostwald ripening process to gradually form regular crystallization [26]. So, with the increase of hydrothermal reaction time, the flakes become larger and thicker.

The TEM images of the synthesized samples are shown in Fig. 4. The NiO microspheres possess an internally porous structure (Fig. 4(a)) and the flakes with clear edges are stacked and crossed to form porous channels (Fig. 4(b)). The magnified image (Fig. 4(b)) shows that the length of flakes is about 400–500 nm and the thickness is about 20–40 nm. These results are consistent with the SEM observations. The selected-area electron diffraction pattern, shown in Fig. 4(c), reveals that the material is composed of polycrystallines with good crystallinity. The (111), (200), (220) and (311) crystal plane structures of NiO are noticeable. The high-resolution TEM image (Fig. 4(d)) demonstrates that the lattice spacings are 0.246 and 0.201 nm, which can be assigned to the (111) and (200) crystal planes of NiO, respectively.

The XRD patterns of hierarchical NiO hollow microspheres and NiO precursor powder are shown in Fig. 5. From the XRD pattern of NiO, the peak is sharp and no impurity peaks were detected, suggesting that the prepared hierarchical NiO hollow microspheres have good purity and crystallinity. The precursor has a high crystallinity, and the diffractions can be readily indexed to pure hexagonal β-Ni(OH)<sub>2</sub> phase (JCPDS No. 14–0117) [27]. After calcination, the NiO precursor has been completely decomposed into NiO. At the same time, due to the repair effect of defects, with the increase of calcination temperature, nonstoichiometric Ni<sub>1-x</sub>O is gradually close to stoichiometric NiO structure [28–30]. The XRD results show that the NiO microspheres possess a cubic texture (PDF card No. 47–1049) [31]. The characteristic diffraction peaks at 2θ=37.2°, 43.27°, 62.88°, 75.41° and 79.4° are attributable to the (111), (200), (220), (311) and (222) crystalline planes, respectively, indicating that purity and crystallinity of the prepared NiO microspheres are perfect.

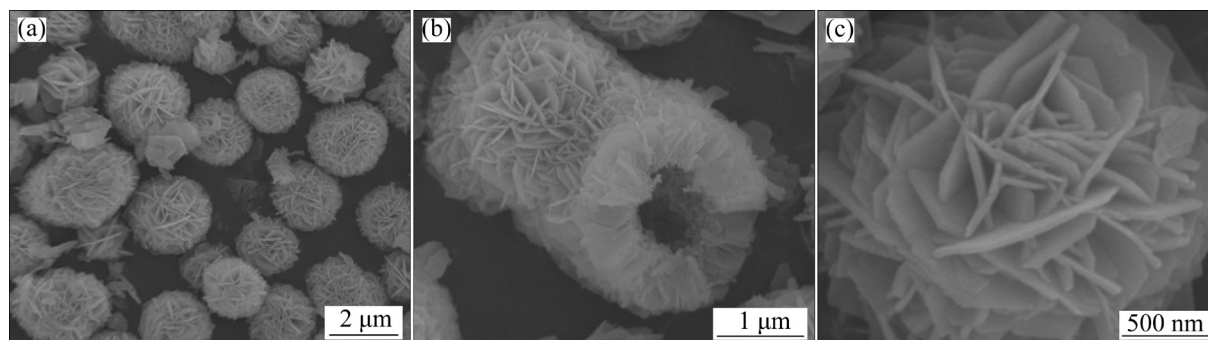
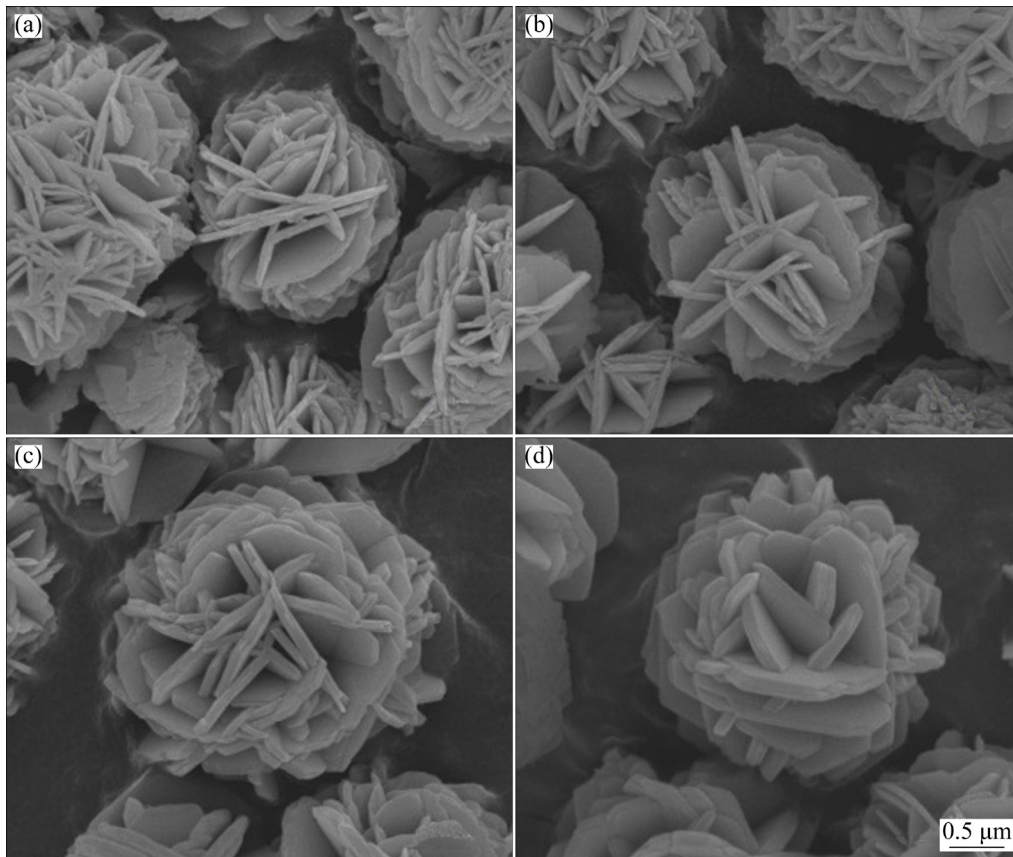
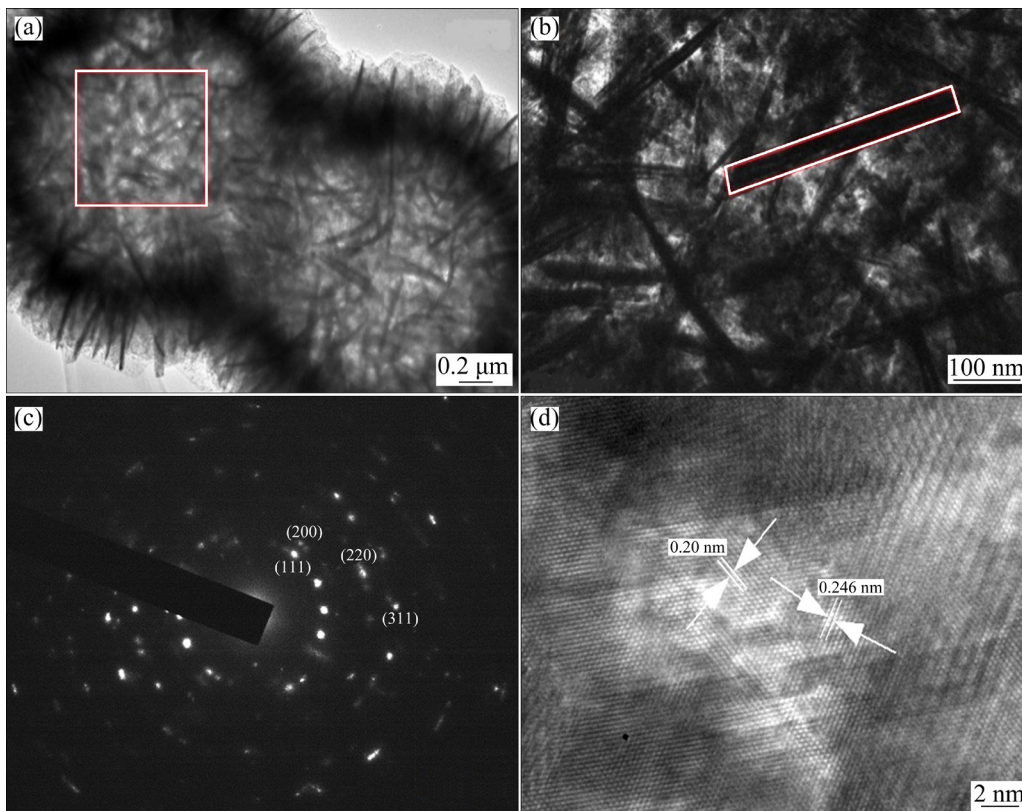


Fig. 2 SEM images of hierarchical NiO hollow microspheres



**Fig. 3** SEM images of NiO microspheres prepared for different hydrothermal reaction time: (a) 6 h; (b) 8 h; (c) 10 h; (d) 12 h



**Fig. 4** TEM images of hierarchical NiO hollow microspheres: (a, b) Morphology of NiO hollow microspheres; (c) Selected-area electron diffraction patterns; (d) High resolution transmission electron image of NiO nanoflakes

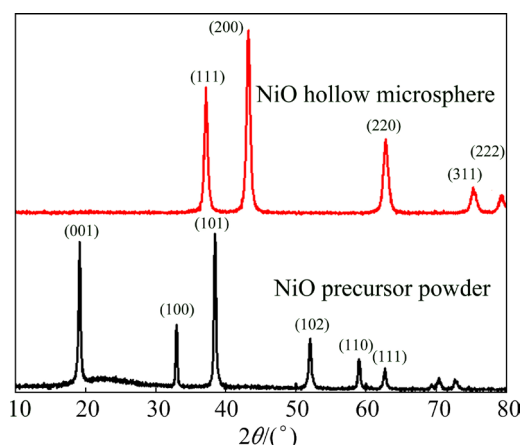


**Fig. 5** XRD patterns of hierarchical NiO hollow microspheres and Ni(OH)<sub>2</sub> precursor powder

The FTIR spectrum for the hierarchical NiO hollow microspheres prepared is shown in Fig. 6. The broad OH<sup>-</sup> stretching band and the bending vibration of hydrogen-bonded water can be seen at 3423 cm<sup>-1</sup> and 1628 cm<sup>-1</sup>, respectively. A relatively weak peak is located at about 418 cm<sup>-1</sup>, in accordance with pure NiO. Although the peak of nickel–oxygen interaction is usually located at about 500 cm<sup>-1</sup> [32], the steric stabilization and surface effects cause its red shift [33].

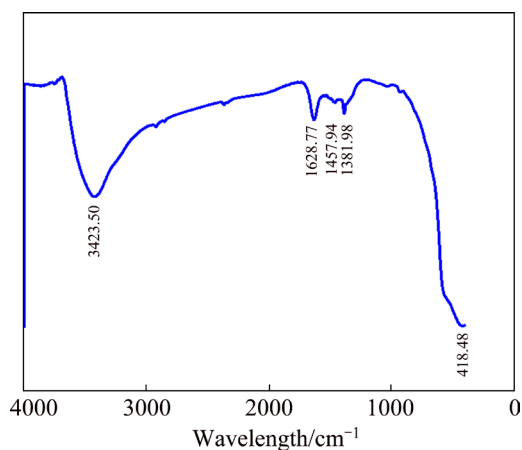
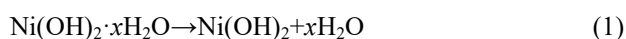


**Fig. 6** FTIR spectrum of hierarchical NiO hollow microspheres

The NiO precursor can decompose to NiO after calcination in air. The thermal behavior of the NiO precursor was investigated with TG–DSC measurements. The resulting curve is shown in Fig. 7. When the temperature is lower than 300 °C, there is a small mass loss associated with the evaporation of adsorbed water according to Eq. (1):



The NiO crystal phase is gradually formed with the removal of the hydroxyl group in Ni(OH)<sub>2</sub> [34]. The major mass loss occurs rapidly between approximately

300 and 400 °C, as shown in the TG curve and by the corresponding sharp exothermic peak in the DSC curve. This process can be explained according to Eq. (2):



There is no obvious mass loss when the temperature is higher than approximately 600 °C, which indicates that the Ni(OH)<sub>2</sub> precursor has decomposed completely to NiO. The total mass loss measured is about 21.4%, in good agreement with the theoretical value (19.4%) calculated from Eq. (2).

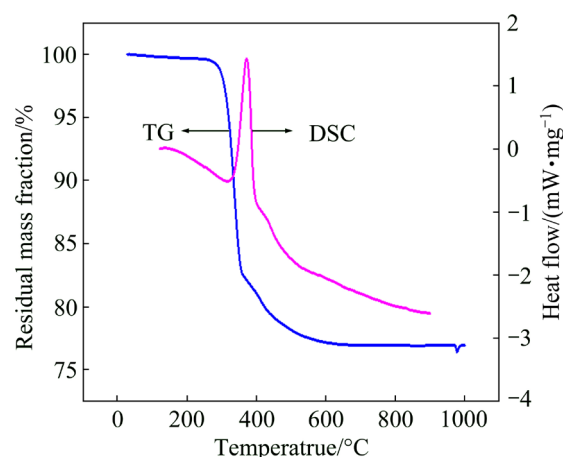


**Fig. 7** TG–DSC curves of precursor of hierarchical NiO hollow microspheres

The information about specific surface and pore structure can be obtained by the N<sub>2</sub> adsorption/desorption isotherm, as shown in Fig. 8. The N<sub>2</sub> adsorption/desorption isotherm presents typical IV-absorption/desorption curve with H4-hysteresis loop at relatively high pressures. In the process, the pores between the NiO sheets are gradually filled by N<sub>2</sub> under the action of capillary force, which makes the adsorption curve deviate from the desorption curve. Correspondingly, the pore structure is a complex network system formed by

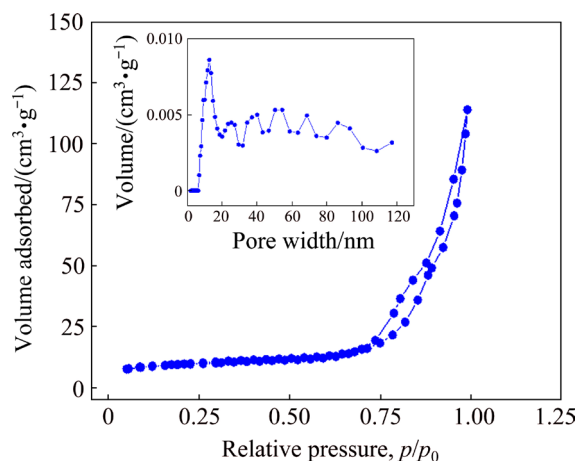


**Fig. 8** N<sub>2</sub> adsorption/desorption isotherm of NiO hollow microspheres (The inset shows the pore size distribution)

the crossing of the straight channel which can demonstrate the presence of holes formed by accumulation of sheets [35]. The BET surface area of NiO hollow microspheres is about 52 m<sup>2</sup>/g. These results are consistent with the SEM observations. The pore size distribution curve indicates that the prepared NiO is a typical mesoporous (2–50 nm) and macroporous (50–500 nm) material, which can benefit the electrolyte infiltrating into the interior of the material and increases the utilization of the active material to improve the electrochemical performance.

A schematic illustration of the fabrication process of the hierarchical NiO hollow microspheres is shown in Fig. 9. When lysine powder is mixed with the NiCl<sub>2</sub> solution, it dissolves into chains and dissociates to zwitterion. The amino group exists in the protonated form, as NH<sub>3</sub><sup>+</sup>, and the carboxylic acid group is present as COO<sup>-</sup>. The chains intertwine and cross-link, similarly to what are usually observed in polymer molecules, to form a 3D skeleton [36]. Ni<sup>2+</sup> is absorbed on the lysine chains because of electrostatic interaction. The chains also provide active sites for Ni<sup>2+</sup> nucleation. The addition of ammonia (NH<sub>3</sub>) brings the pH value of the mixture solution to be about 13, which is far greater than the isoelectric point of lysine (9.74) [37]. The hydrolysis reaction of NH<sub>3</sub> can provide OH<sup>-</sup> ions, which combine with Ni<sup>2+</sup> to form Ni(OH)<sub>2</sub> flakes, according to Eqs. (4) and (6). In addition, as shown in Eqs. (3) and (5), NH<sub>3</sub> can form a complex with Ni<sup>2+</sup> ions, decreasing the concentration of free Ni<sup>2+</sup> and consequently reducing the

growth rate of the crystals [38]. The growth of some crystal planes can be inhibited by the absorption of lysine on the nucleation surface [39], which results in the formation of the flakes. The precursors of NiO microspheres can be formed through a self-assembling growth process and usually present a good dispersion and uniform size because of the steric hindrance and bridge function of the lysine chains. After calcination, lysine can be removed and Ni(OH)<sub>2</sub> is decomposed completely into NiO, resulting in the formation of black NiO hollow microspheres.



### 3.2 Electrochemical evaluation

The conductive mechanism of NiO used as an electrode material has not been clearly reported. Here, we studied its conductive mechanism, which is realized by electron transmission and holes trapping ions. Conduction is a diffusion balance process of electrons, holes and ions in the NiO lattice, which realizes the continuous component change of the active substance from completely charged state of NiOOH to completely discharged state of NiO. The electrode reaction equation of NiO can be expressed by [40]

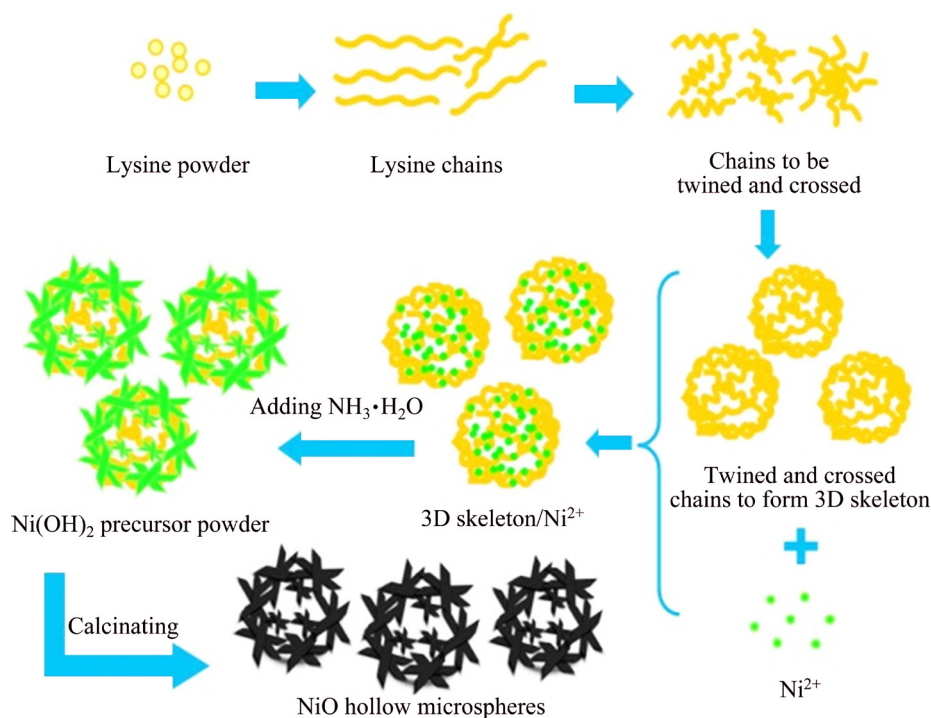


Fig. 9 Schematic illustration of synthesis of hierarchical NiO hollow microspheres

$\text{Ni}^{3+}$  lacks one electron compared to  $\text{Ni}^{2+}$ , which is referred to as an electron defect and simultaneously generates a hole [41]. Since the stoichiometric NiO materials are difficult to prepare, NiO products with few  $\text{Ni}^{3+}$  and holes can be usually obtained, which behave as electron defects and hole defects [42]. The redox reactions, occurring at the interface between electrode and electrolyte, are realized by the transformation of electron defects and hole defects, capturing  $\text{OH}^-$ . Figure 10 shows a schematic diagram of the migration of reactive particles during the charging process of NiO electrodes.

During the anodic oxidation process,  $\text{O}^{2-}$  in the crystal lattice and  $\text{H}^+$  in the solution are aligned to form a double layer at the solid/liquid interface [41]. The conversion from  $\text{Ni}^{2+}$  to  $\text{Ni}^{3+}$  creates an electron, which is transferred to the current collector, entering external circuit. At the same time, the holes move out of the NiO crystal lattice and  $\text{OH}^-$  ions cross the interface into the NiO bulk phase [43].  $\text{OH}^-$  ions can be trapped by the holes in the process. As a result, there are electron defects and  $\text{OH}^-$  ions trapped by holes in the solid phase, as shown in Fig. 10(b). Since the holes in the surface are exhausted by trapping the  $\text{OH}^-$  ions, they are less numerous than those in the bulk phase. Such a concentration gradient causes the holes to diffuse from the bulk to the surface of the NiO crystal; however, the diffusion rate is lower than the reaction rate, causing the concentration of holes in the surface to decrease, thus reducing the surface potential of the electrode [44]. As a result, the voltage must increase to sustain the reaction.

The cathodic reduction process is opposite to the anodic oxidation process.  $\text{Ni}^{3+}$  is converted to  $\text{Ni}^{2+}$  when combining an electron from the external circuit, which reduces holes concentration and causes the holes to move towards the bulk from the surface while  $\text{OH}^-$  ions cross the interface into the solution.

Figure 11 shows the CV curves of hierarchical

structure of NiO hollow microspheres at different scan rates in a 6 mol/L KOH aqueous solution. The curves exhibit a pair of electrochemical redox peaks in the potential range from  $-0.05$  to  $0.55$  V.

The CV curves have a pair of redox peaks, which correspond to the faradic oxidation/reduction reactions. The oxidation peak at about  $0.3$  V is due to the NiO conversion to NiOOH, whereas the reduction peak at about  $0.08$  V is due to the reverse reaction. In addition, the oxidation and reduction peaks are symmetrical, indicating good reversibility of the redox reactions occurring at, or near, the porous microsphere surfaces [45]. The polarization of the electrode increases with the scanning rate and leads to an increase of the internal resistance, which makes the oxidation peak potential shift in the positive direction and the reduction peak potential shift in the negative direction, correspondingly. At the same time, the redox peaks become less clear as the scan rate increases because there is not enough time for the transportation of electrons and electrolyte ions.

Galvanostatic charge–discharge curves of hierarchical structure of NiO hollow microspheres at different current densities in 6 mol/L KOH aqueous solution are shown in Fig. 12. The specific capacitance can be calculated from charge/discharge curves according to Eq. (8):

$$C = \frac{I\Delta t}{mV} \quad (8)$$

where  $I$  is the applied current (A),  $\Delta t$  is the discharge time (s),  $V$  is the potential window (V), and  $m$  is the mass (g) of the NiO active material.

It can be seen from Fig. 12 that the charging and discharging time of NiO electrode material decreases with the increase of current density. The reason is that when the current density increases, a lot of electrolyte ions are adsorbed on the electrode surface in a short period of time, which reduces the diffusion rate of ions in

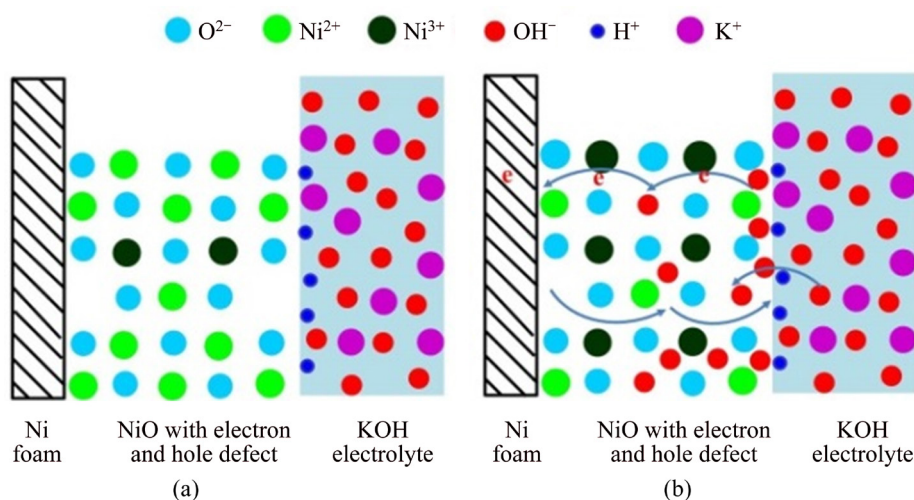
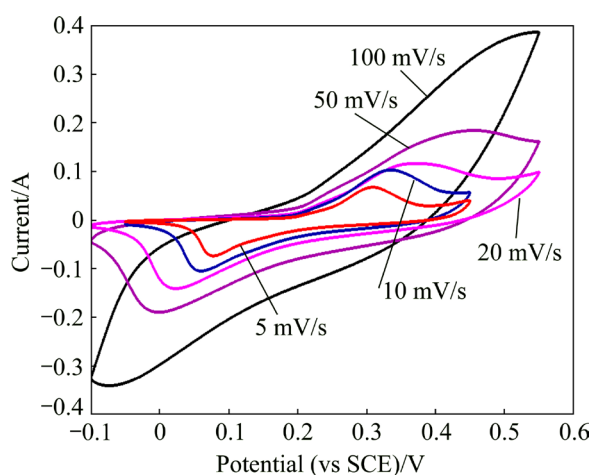
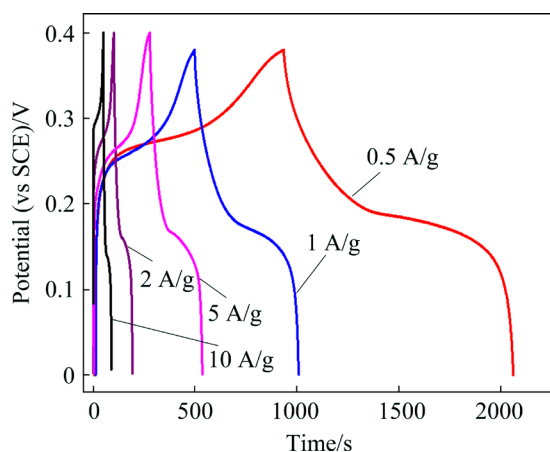


Fig. 10 Schematic diagram of migration of reactive particles during charging process: (a) Primitive state; (b) Anodic oxidation state



**Fig. 11** CV curves of hierarchical structure of NiO hollow microspheres at scan rates of 5, 10, 20, 50 and 100 mV/s in 6 mol/L KOH solution



**Fig. 12** Galvanostatic charge-discharge curves of hierarchical NiO hollow microspheres at current densities of 0.5, 1, 2, 5 and 10 A/g in 6 mol/L KOH solution

the electrolyte. As a result, electrolyte ion concentration at the solid/liquid interface decreases rapidly. At the same time, the number of charging ions on the electrode is less than the required, so the polarization effect caused by the liquid phase diffusion on the electrode increases, and with the reaction, the step becomes the control step. Therefore, the charging and discharging time is shortened, and the capacitance value is decreased [46–48].

The specific capacitance values of the prepared NiO samples are 1482 and 1340 F/g at discharge density of 0.5 and 1 A/g, respectively, according to Fig. 12. Since the electrolyte can completely infiltrate into the interior of the NiO material, the electrons and electrolyte ions have enough time to diffuse. The long discharge time of the curves suggests the outstanding electrochemical performance of NiO. On one hand, the hierarchical NiO hollow microspheres present high porosity and good

diffusion channels, which are beneficial to the diffusion and migration of both electrolyte ions and electrons; on the other hand, the Ni foam used as a current collector has good electrical conductivity. Consequently, the specific capacitance is greatly improved.

The galvanostatic charge-discharge curves of hierarchical structure NiO hollow microspheres synthesized using different hydrothermal reaction time are shown in Fig. 13. According to Eq. (8), after hydrothermal reaction time treatment for 6, 8, 10 and 12 h, the specific capacitance values of the prepared NiO samples are 1340, 1003, 855 and 766 F/g at 1 A/g, respectively. As mentioned previously, the NiO flakes grow along the face-direction with increasing hydrothermal treatment time, which effectively decreases the contact surface area between NiO and the electrolyte as well as reduces the conductivity of the electrode.

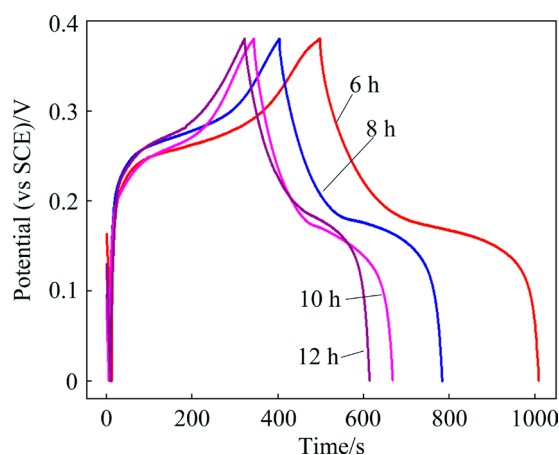


**Fig. 13** Galvanostatic charge-discharge curves of NiO microspheres obtained with different hydrothermal reaction time at current density of 1 A/g in 6 mol/L KOH solution

The electrochemical performance was further investigated through EIS measurements. The results are shown in Fig. 14.

The curve is composed of an arc in the high frequency region and a line in the low frequency region. The intercept with the real axis at high frequency reflects the resistance of the solution ( $R_s$ ), whose value is about 0.54  $\Omega$ . The semicircle in the high frequency region is related to the charge transfer resistance ( $R_{ct}$ ) of about 4.46  $\Omega$ , and the straight line indicates the diffusion resistance (Warburg impedance,  $W$ ) of the electrolyte in electrode pores and the  $\text{OH}^-$  ions diffusion in the host material [32]. The fitting curve, based the on equivalent circuit, is also shown in the inset of Fig. 14. Here,  $C_F$  is the Faradaic pseudo capacitor, and  $C_d$  is double-layer capacitance.

One of the important requirements for supercapacitor application is a long cycling life [49]. So, cycling galvanostatic charge/discharge tests were further

performed to evaluate the stability of the hierarchical NiO hollow microspheres materials. The cycle performance and the capacitance retention are shown in Fig. 15. After 1000 cycles, the capacity retention rate of the prepared microspheres is 96.5%, which shows a good cyclic stability. Thanks to its unique hierarchical hollow structure, the electrolyte ions ( $\text{OH}^-$ ) are more likely to prolapse and be embedded in the reasonable pore size distribution and interconnected channels during the circulation process, which can improve the utilization rate of active substance NiO and make NiO electrode materials have low attenuation capacity.

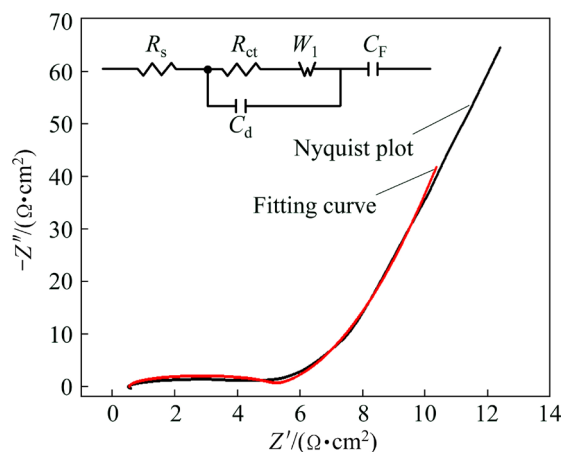


Fig. 14 Nyquist plots of hierarchical NiO hollow microspheres electrode (The inset shows the equivalent electrical circuit)

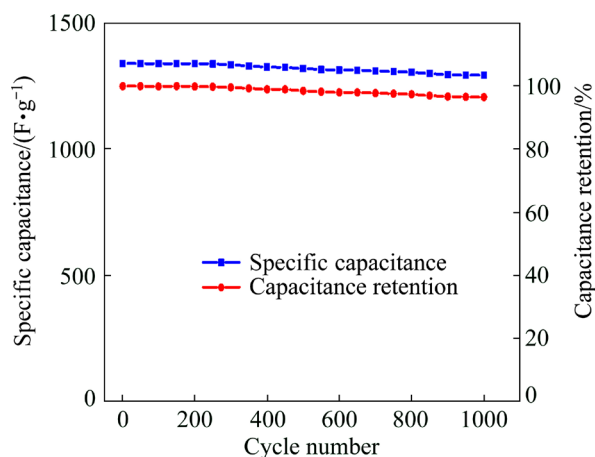


Fig. 15 Cycle performance and capacitance retention of prepared hierarchical NiO hollow microspheres

## 4 Conclusions

1) The hierarchical NiO hollow microspheres with high porosity and specific surface area as well as open channels were prepared through self-assembling, hydrothermal reaction and calcination with the help of Lysine used as a structure regulator.

2) The conductive mechanism, realized by electron and hole trapping ions, was investigated. The process can

realize the continuous change of the active substance component from the completely charged state of NiOOH to the completely discharged state of NiO.

3) The hierarchical NiO hollow microspheres have good electrochemical capacitive performance, providing an excellent specific capacitance of 1340 F/g at a current density of 1 A/g and having high capacitance retention about 96.5% after 1000 cycles.

## References

- [1] ZHAO Qing-lan, WANG Xian-you, JIANG Lan-lan, WU Hao, WU Chun. Preparation and supercapacitive characteristics of new carbon materials derived from furfuryl alcohol [J]. The Chinese Journal of Nonferrous Metals, 2013, 23: 1977–1984. (in Chinese)
- [2] WANG Hai-liang, CASALONGUE H S, LIANG Yong-ye, Dai Hong-jie. Ni(OH)<sub>2</sub> nanoplates grown on graphene as advanced electrochemical pseudocapacitor materials [J]. Journal of the American Chemical Society, 2010, 132: 7472–7477.
- [3] BAO Li-hong, ZANG Jian-feng, LI Xiao-dong. Flexible Zn<sub>2</sub>SnO<sub>4</sub>/MnO<sub>2</sub> core/shell nanocable-carbon microfiber hybrid composites for high-performance supercapacitor electrodes [J]. Nano Letters, 2011, 11: 1215–1220.
- [4] ZHU Yi-rong, JI Xiao-bo, PAN Chen-chi, SUN Qing-qing, SONG Wei-xin. A carbon quantum dot decorated RuO<sub>2</sub> network: Outstanding supercapacitances under ultrafast charge and discharge [J]. Energy & Environmental Science, 2013, 6: 3665–3675.
- [5] HU Ying-ying, HU Zhong-ai, ZHANG Ya-jun, LU Ai-lian, XU Huang, ZHANG Zi-yu. Synthesis and electrochemical characterization of RuO<sub>2</sub>·xH<sub>2</sub>O/graphite nanosheet composite array electrodes for supercapacitors [J]. Acta Physico-Chimica Sinica, 2013, 29: 305–310.
- [6] VELLACHERI R, PILLAI V K, KURUNGOT S. Hydrrous RuO<sub>2</sub>-carbon nanofiber electrodes with high mass and electrode-specific capacitance for efficient energy storage [J]. Nanoscale, 2012, 4: 890–896.
- [7] LEE J W, AHN T, KIM J H. Nanosheets based mesoporous NiO microspherical structures via facile and template-free method for high performance supercapacitors [J]. Electrochimica Acta, 2011, 56: 4849–4857.
- [8] TIAN Xian-qing, CHENG Chang-ming, QIAN Lei, ZHENG Bao-zhan. Microwave-assisted non-aqueous homogenous precipitation of nanoball-like mesoporous α-Ni(OH)<sub>2</sub> as a precursor for NiO<sub>x</sub> and its application as a pseudocapacitor [J]. Journal of Materials Chemistry, 2012, 22: 8029–8035.
- [9] ZHANG Bing-jie, LI Wen-yao, SUN Jian-qing, He Guan-jie, CHEN Zhi-gang. NiO/MnO<sub>2</sub> core/shell nanocomposites for high-performance pseudocapacitors [J]. Materials Letters, 2014, 114: 40–43.
- [10] SAHA S, CHHETRI S, KHANRA P, SAMANTA P, KOO H. In-situ hydrothermal synthesis of MnO<sub>2</sub>/NiO@Ni hetero structure electrode for hydrogen evolution reaction and high energy asymmetric supercapacitor applications [J]. Journal of Energy Storage, 2016, 5: 22–31.
- [11] SUN Qiang-qiang, BAO Shu-juan. Effects of reaction temperature on microstructure and advanced pseudocapacitor properties of NiO prepared via simple precipitation method [J]. Nano-Micro Letters, 2013, 5: 289–295.
- [12] TANG Yong-fu, LIU Yan-yan, YU Sheng-xue, GUO Wan-chun, MU Shi-chun, WANG Hong-chao, GAO Fa-ming. Template-free hydrothermal synthesis of nickel cobalt hydroxide nanoflowers with high performance for asymmetric supercapacitor [J]. Electrochimica Acta, 2015, 161: 279–289.

- [13] DAI Kai, LIANG Chang-hao, DAI Jian-ming, LU Lu-hua, ZHU Guang-ping. High-yield synthesis of carbon nanotube-porous nickel oxide nanosheet hybrid and its electrochemical capacitance performance [J]. *Materials Chemistry & Physics*, 2014, 143: 1344–1351.
- [14] LV Yao-hui, HUANG Kai, ZHANG Wei, RAN Song-lin, CHI Fang-li. High-performance gas-sensing properties of octahedral NiO crystals prepared via one-step controllable synthesis route [J]. *Crystal Research & Technology*, 2014, 49: 109–115.
- [15] WANG Chun-dong, XU Jun-ling, ZHANG Jie, ZHANG Wei-jun. Hierarchical composite electrodes of nickel oxide nanoflake graphene for high-performance pseudocapacitors [J]. *Advanced Functional Materials*, 2014, 24: 6372–6380.
- [16] LI Guo-chang, LIU Peng-fei, LIU Rui, LIU Min-min, HAN Lei. MOF-derived hierarchical double-shelled NiO/ZnO hollow spheres for high-performance supercapacitors [J]. *Dalton Transactions*, 2016, 45: 13311–13316.
- [17] ZHANG Xiao-jun, SHI Wen-hui, ZHU Ji-xin, YAN Qing-yu. Synthesis of porous NiO nanocrystals with controllable surface area and their application as supercapacitor electrodes [J]. *Nano Research*, 2010, 3: 643–652.
- [18] VIJAYAKUMAR S, NAGAMUTHU S, MURALIDHARAN G. Supercapacitor studies on NiO nanoflakes synthesized through a microwave route [J]. *ACS Applied Materials & Interfaces*, 2013, 5: 2188–2196.
- [19] YEAGER M P, SU D, MARINKOVIC N S. Pseudocapacitive NiO fine nanoparticles for supercapacitor reactions [J]. *Journal of The Electrochemical Society A*, 2012, 159: 1598–1603.
- [20] KIM S I, LEE J S, AHN H J. Facile route to an efficient NiO supercapacitor with a three-dimensional nanonetwork morphology [J]. *ACS Applied Materials & Interfaces*, 2013, 5: 1596–1603.
- [21] ZHU Jian-hui, JIANG Jian, LIU Jing-ping, HUANG Xin-tang. Direct synthesis of porous NiO nanowall arrays on conductive substrates for supercapacitor application [J]. *Journal of Solid State Chemistry*, 2011, 184: 578–583.
- [22] BELLO A, MAKGOPA K, FABIANE M. Chemical adsorption of NiO nanostructures on nickel foam-graphene for supercapacitor applications [J]. *Journal of Materials Science*, 2013, 48: 6707–6712.
- [23] WU Chun-hui, DENG Si-hui, WANG Hao, YAN Hui, LIU Jing-bing. Preparation of novel three-dimensional NiO/ultrathin derived graphene hybrid for supercapacitor applications [J]. *ACS Applied Materials & Interfaces*, 2014, 6: 1106–1112.
- [24] HUANG Zhi-xiang, WANG Ye, SHI Wen-hui, YANG Hui-ying. Synthesis of self-assembled cobalt sulphide coated carbon nanotube and its superior electrochemical performance as anodes for Li-ion batteries [J]. *Electrochimica Acta*, 2015, 167: 388–395.
- [25] LI Xia, LIU Gui-xia, DONG Xiang-ting, WANG Jin-xian. Research progress for various morphologies of nanomaterials with amino acids-assisted synthesis [J]. *Chemistry*, 2011, 74: 325–332.
- [26] YAO Ming-ming, HU Zhong-hua, XU Zi-jie, LIU Ya-fei, ZHANG Qiang. High-performance electrode materials of hierarchical mesoporous nickel oxide ultrathin nanosheets derived from self-assembled scroll-like alpha-nickel hydroxide [J]. *Journal of Power Sources*, 2015, 273: 914–922.
- [27] WANG YAN, GAI Shi-li, LI Chun-xia, ZHANG Mi-lin, YANG Piao-ping. Controlled synthesis and enhanced supercapacitor performance of uniform pompon-like  $\beta$ -Ni(OH)<sub>2</sub> hollow microspheres [J]. *Electrochimica Acta*, 2013, 90: 673–681.
- [28] BAGGETTO L, DUDNEY N J, VEITH G M. Surface chemistry of metal oxide coated lithium manganese nickel oxide thin film cathodes studied by XPS [J]. *Electrochimica Acta*, 2013, 90: 135–147.
- [29] LIANG Kun, TANG Xian-zhogn, HU Wen-cheng. High-performance three-dimensional nanoporous NiO film as a supercapacitor electrode [J]. *Journal of Materials Chemistry*, 2012, 22: 11062–11067.
- [30] CAO Pei-qi, WANG Lin-cai, XU Yan-jie, FU Yan-bao, MA Xiao-hui. Facile hydrothermal synthesis of mesoporous nickel oxide/reduced graphene oxide composites for high performance electrochemical supercapacitor [J]. *Electrochimica Acta*, 2015, 157: 59–68.
- [31] TRUNG N B, TAM T V, DANG D K, BABU K F. Facile synthesis of three-dimensional graphene/nickel oxide nanoparticles composites for high performance supercapacitor electrodes [J]. *Chemical Engineering Journal*, 2015, 264: 603–609.
- [32] MARICHI R B, SAHU V, LALWANI S, SHARMA R K. Nickel-shell assisted growth of nickel-cobalt hydroxide nanofibres and their symmetric/asymmetric supercapacitive characteristics [J]. *Journal of Power Sources*, 2016, 325: 762–771.
- [33] SONAVANE A C, INAMDAR A I, SHINDE P S. Efficient electrochromic nickel oxide thin films by electrodeposition [J]. *Journal of Alloys & Compounds*, 2010, 489: 667–673.
- [34] ABDALLA A M, SAHU R P, WALLAR C J, CHEN R, ZHITOMIRSKY I. Nickel oxide nanotube synthesis using multiwalled carbon nanotubes as sacrificial templates for supercapacitor application [J]. *Nanotechnology*, 2017, 28: 075603.
- [35] ZHENG Ming-tao, ZHANG Hao-ran, GONG Xue-bin, XU Ru-chun, XIAO Yong. A simple additive-free approach for the synthesis of uniform manganese monoxide nanorods with large specific surface area [J]. *Nanoscale Research Letters*, 2013, 8: 166–172.
- [36] YANG Xiao-deng, SHEN Qiang, XU Gui-yang. Crystallization of calcium carbonate using water-soluble macromolecules [J]. *Acta Physico-Chimica Sinica*, 2010, 26: 2087–2095.
- [37] JADHAV H S, THORAT G M, MUN J, SEO J G. Self-assembled hierarchical NiO microspheres with ultra-thin porous nanoflakes for lithium-ion batteries [J]. *Journal of Power Sources*, 2016, 302: 13–21.
- [38] JIANG Hao, ZHAO Ting, LI Chun-zhong, MA Jian. Hierarchical self-assembly of ultrathin nickel hydroxide nanoflakes for high-performance supercapacitors [J]. *J Mater Chem*, 2011, 21: 3818–3823.
- [39] REN Li-ying, ZHANG Qun, ZHU Wan-hua, LI Qian-qian. Biomimetic synthesis of CaCO<sub>3</sub> microrings [J]. *Journal of Synthetic Crystals*, 2015, 44: 250–255. (in Chinese)
- [40] ZULKIFLI R, DERAMAN M, DAIK R, SULEMAN M. Electrochemical characterization of supercapacitor electrodes prepared by activation of green monoliths consist of self-adhesive carbon grains and lignin [J]. *Materials Science Forum*, 2016, 846: 545–550.
- [41] KUMAR R, SINGH R K, SAVU R, DUBEY P K, KUMAR P. Microwave-assisted synthesis of void-induced graphene-wrapped nickel oxide hybrids for supercapacitor applications [J]. *RSC Advances*, 2016, 6: 26612–26620.
- [42] ZHANG Yi-dong, LI Zhi-wei. Low-temperature fabrication of sol-gel NiO film for optoelectronic devices based on the ‘fuel’ of urea [J]. *Ceramics International*, 2016, 42: 6360–6368.
- [43] CHEN Nan, LI Qing, LI Yu-xiu, DENG Dong-yang, XIAO Xue-chun, WANG Yu-de. Facile synthesis and gas sensing performances based on nickel oxide nanoparticles/multi-wall carbon nanotube composite [J]. *Journal of Materials Science: Materials in Electronics*, 2015, 26: 8240–8248.
- [44] COM B J M B. Influence of TiO on the electrochemical performance of pasted type -nickel hydroxide electrode in alkaline electrolyte [J]. *Journal of Natural Gas Chemistry*, 2016, 25: 41–48.
- [45] KIM J H, ZHU K, YAN Y. Microstructure and pseudocapacitive properties of electrodes constructed of oriented NiO–TiO<sub>2</sub> nanotube arrays [J]. *Nano Letters*, 2010, 10: 4099–4104.
- [46] ZHOU Guang-min, WANG Da-wei, FENG Li, ZHANG Li-li, WENG Zhe. The effect of carbon particle morphology on the electrochemical properties of nanocarbon/polyaniline composites in

- supercapacitors [J]. *New Carbon Materials*, 2011, 26: 180–186.
- [47] HALL P J, MIRZAEIAN M, FLETCHER S I, SILLARS F B, RENNIE A J R. Energy storage in electrochemical capacitors: Designing functional materials to improve performance [J]. *Energy & Environmental Science*, 2010, 3: 1238–1251.
- [48] YE H, CHENG Y, HOBSON T. Design and synthesis of hierarchical MnO<sub>2</sub> nanospheres/carbon nanotubes/conducting polymer ternary composite for high performance electrochemical electrodes [J]. *Nano Letters*, 2010, 10: 2727–2733.
- [49] SEN P, DE A, CHOWDHURY A D, BANDYOPADHYAY S K. Conducting polymer based manganese dioxide nanocomposite as supercapacitor [J]. *Electrochimica Acta*, 2013, 108: 265–273.

## 具有高赝电容的微纳分级 NiO 中空微球的可控制备

杨洪志, 邹俭鹏

中南大学 粉末冶金国家重点实验室, 长沙 410083

**摘要:** 采用水热合成-煅烧的方法, 通过自组装过程, 制备具有微纳分级结构的 NiO 中空微球。所制备的微纳分级结构 NiO 微球由许多 NiO 纳米片相互堆叠而成, 颗粒粒径大约为 2~3 μm。NiO 纳米片边缘清晰, 片长约为 500~700 nm, 厚度仅为 40~50 nm。这种独特的微纳分级结构使得 NiO 材料具有相互贯通的孔道, 这有利于电解质离子和电子的扩散和迁移。所制备的微纳分级结构 NiO 电极材料具有优越的电化学性能, 在 1 A/g 的电流密度下比电容可达到 1340 F/g, 且循环 1000 次后, 容量保持率为 96.5%。同时, 对氧化镍电化学电容器的导电机理进行探究。

**关键词:** 氧化镍中空微球; 微纳分级结构; 可控制备; 自组装; 赝电容

(Edited by Bing YANG)